Evaluation method of transit time difference for clamp-on ultrasonic flowmeters in two-phase flows

Murakawa, Hideki ; Ichimura, Shuhei ; Sugimoto, Katsumi ; Asano, Hitoshi ; Umezawa, Shuichi ; Sugita, Katsuhiko

(Citation)
Experimental Thermal and Fluid Science,112:109957

(Issue Date)
2020-04-01

(Resource Type)
journal article

(Version)
Accepted Manuscript

(URL)
https://hdl.handle.net/20.500.14094/90006822

Highlights:

- Standard deviation of the signal was proposed for TOF calculation at lower SNRs
- Guided wave is the dominant effect for reducing SNR of the target signal
- Guided wave is strongly influenced by fluctuation of liquid film
- Success ratio of TOF measurements depends on the flow regime in two-phase flow
- Distribution of the standard deviation can be used for the flow regime estimation

Evaluation method of transit time difference for clamp-on ultrasonic flowmeters in two-phase flows

Hideki Murakawa*[1], Shuhei Ichimura[1], Katsumi Sugimoto[1], Hitoshi Asano[1], Shuichi Umezawa[2], Katsuhiko Sugita[2]

[1] Department of Mechanical Engineering, Graduate School of Engineering, Kobe University, 1-1 Rokkodai, Nada, Kobe 657-8501, Japan

[2] Tokyo Electric Power Company Holdings, Inc., 4-1 Egasaki, Tsurumi, Yokohama 230-8510, Japan

*E-mail: murakawa@mech.kobe-u.ac.jp

Abstract

To achieve efficient energy management in industrial plants, it is crucial to measure the steam flow rates at the various points of consumption. Clamp-on time-of-flight ultrasonic flowmeters are useful devices to measure the steam flow rates in existing pipes. However, it is difficult to accurately measure the steam flow rates because of the large acoustic impedance difference between the pipe material and fluid, strong signal attenuation in the fluid, and high temperature. In addition, the steam wetness increases with heat losses and the presence of liquid film and droplets that creates noise in the detected ultrasonic signals, making it difficult to distinguish the target signals from the noisy ones. Hence, a new signal processing method is proposed to determine the transit time difference, particularly at lower signal-to-noise ratios. Two ultrasonic transducers were used to measure the ultrasonic time-of-flight, which varies depending on the flow rate. The transmitted ultrasonic signals were time-dependent due to the generation of guided waves in the pipe wall. The standard deviations of the target signals increased when the flow regime transitioned from stratified to annular mist flow. The guided waves significantly influence the success ratio of determining the transit time difference between the ultrasonic

signals transmitted from the upstream and downstream transducers. Based on the results, the use of the standard deviation of the target signals is proposed for estimating the transit time difference. Further, as the standard deviation varied significantly depending on the flow regime, it can be used to identify the flow regime as well.

Keywords: ultrasonic signal propagation, clamp-on, time-of-flight flowmeter, guided waves, steam flow rate, two-phase flow

1. Introduction

In modern times, most of the heat demands are supplied by steam in industrial plants. Saturated steam is generated in boilers, which is then supplied through a piping system. Even though the steam flow rate is controlled at the boilers, the actual steam flow rates at different points of consumption may vary when condensation occurs as the steam flows through the piping system because of the heat loss. As a result, saturated steam flow may change to two-phase flow such as stratified, wavy and annular-mist flows. Hence, it is essential to monitor the wet steam flow rate at each point of consumption to achieve efficient energy management. In particular, orifice, vortex, and in-line ultrasonic flowmeters are typically used to measure the gas or steam flow rates [1]. Even though a number of studies have been carried out to measure wet steam flow rates [2], these flowmeters must be connected to the pipes and it is difficult to install them in existing pipes. One of the effective solutions to measure the steam flow rates in existing pipes is to use clamp-on ultrasonic flowmeters.

Ultrasonic flowmeters have been developed for more than 60 years and these instruments are widely used to measure the flow rates in liquid and gas flows [3]. There are two types of ultrasonic flowmeters based on their operating principle: (1) pulsed and continuous-wave Doppler ultrasonic flowmeters [4–8] and (2) time-of-flight (TOF) ultrasonic flowmeters. TOF ultrasonic flowmeters

calculate the transit time of the ultrasonic signal between the downstream and upstream sensors, which is influenced by the line-averaged velocity along the ultrasonic beam. TOF ultrasonic flowmeters can be further classified as in-line and clamp-on types based on the sensor settings. For in-line TOF ultrasonic flowmeters, the ultrasonic sensors are installed at designated points within the piping system. In contrast, for clamp-on TOF ultrasonic flowmeters, the ultrasonic sensors are installed at designated points external to the piping system. The ultrasonic sensors are removable in this case, which makes it more convenient to measure the gas or liquid flow rates at various points of consumption in the piping system.

Many studies have been carried out to devise methods in order to improve gas and steam flow rate measurements using ultrasonic flowmeters. Kurniadi and Trisnobudi [9] developed a method to measure the two-dimensional velocity profiles of gas flows using ultrasonic tomography based on the transit time. Shen [10] proposed a method to evaluate the steam quality using a TOF ultrasonic flowmeter, and the results showed that the accuracy of the evaluation was influenced by the wetness of the steam. Xing et al. [11] proposed a correction method for flow rate measurements of two-phase (liquid–gas) flows in a horizontal pipe under stratified and annular flow regimes. However, these studies are focused on in-line ultrasonic flowmeters and most of the studies pertaining to clamp-on ultrasonic flowmeters are focused on liquid flows. The intensity of the transmitted ultrasonic signal tends to decrease in gas flows because the signal attenuation is more pronounced in gas than that in liquid. The significant difference in acoustic impedance between the pipe material and gas also contributes to the

lower intensity of the transmitted ultrasonic signal. To suppress the noise waves arising from the significant acoustic impedance between the pipe material and gas, Nishiguchi et al. [12] proposed a method to measure the gas flow rate at low-pressure conditions (< 0.06 MPa) using ultrasonic transducers designed to follow the curvature of the pipe and a polystyrene wedge attached to the external surface of the pipe wall.

In addition to the acoustic impedance difference, the high temperature of the pipe and wetness of the steam are also critical factors that affect steam flow rate measurements. The sensitivity of the piezoelectric elements in the ultrasonic sensors tends to decrease with an increase in temperature. The wetness of the steam tends to vary because of heat losses, which affects the characteristics of the ultrasonic signal propagation. All of these factors pose a significant challenge to obtaining accurate steam flow rate measurements using clamp-on ultrasonic flowmeters. Sasaki and Hayashi [13] and, Hayashi et al. [14] developed an ultrasonic sensor in which the incidence angle of the ultrasonic signal was 57°. The angle between the wedge and pipe surface was greater than the critical angle. Therefore, ultrasonic wave does not propagate into the pipe wall as a body wave *i.e.* share wave. However, the ultrasonic signals transmitted through the gas flow resulted in higher signal-to-noise ratios (SNRs). Lamb wave has been widely used for measuring gas flowrates [15]. The Lamb wave produces a wider

beam and offers formidable resistance against the effect of suspended solids and droplets [16]. Sasaki et al. [17] developed a damping material to reduce the reflected propagated waves in the pipe wall and found that it was possible to measure the steam flow rates using the ultrasonic sensors and damping material. Morita et al. [18, 19] obtained accurate steam flow rates for stratified and wavy flows but they found that it was difficult to obtain accurate measurement for annular mist flows.

The steam flow rate is directly related to the transit time difference of the ultrasonic signals transmitted from the upstream and downstream transducers. The transmitted ultrasonic signals are prone to noise. The presence of liquid films and droplets due to the steam wetness may alter the propagation paths of the ultrasonic signals emitted from the transducers, leading to noisy signals. Fluctuations at the liquid-gas interface also leads to signal reflections and some of the reflected signals are transmitted through the pipe wall as guided waves. This creates noise in the detected ultrasonic signals, making it difficult to distinguish the target signals from the noisy ones and thus, it is not possible to accurately determine the transit time difference and steam flow rate. To address these issues, the objective of this study is to develop a new signal processing method to determine the transit time difference, particularly at lower SNRs. Experiments were carried out for air–water two-phase flows in a horizontal pipe. The

standard deviations of the transmitted ultrasonic signals are newly proposed for the TOF analysis. The transmitted ultrasonic signals and their standard deviations were compared for stratified, wavy, and annular mist flows in order to determine the relationship between the flow regime and transmitted ultrasonic signals.

2. Time-of-flight ultrasonic flowmeter

Fig. 1 shows the schematic of a TOF ultrasonic flowmeter. The flowmeter consists of a pair of ultrasonic transducers installed upstream and downstream at the external surface of the pipe. Each ultrasonic transducer consists of a piezoelectric element inclined at an angle such that the incidence angel of the ultrasonic signal is α. If an ultrasonic pulse is emitted from the upstream transducer, the transit time of the ultrasonic signal, T_1, is reduced depending on the flow velocity whereas the transit time of the ultrasonic signal from the downstream transducer, T_2, is increased. The transit time of the ultrasonic signal from the upstream and downstream transducers can be determined from the following equations:

$$\begin{aligned} T_1 &= \left(D/\cos\theta\right)/\left(c_\mathrm{f} + V_\mathrm{L}\sin\theta\right) + t_0 \\ T_2 &= \left(D/\cos\theta\right)/\left(c_\mathrm{f} - V_\mathrm{L}\sin\theta\right) + t_0 \end{aligned}, \tag{1}$$

where D is the inner diameter of the pipe; θ is the refraction angle of the ultrasonic signal measured with respect to the flow normal; c_f is the speed of sound in the fluid; V_L is the line-averaged velocity; and t_0

is the transit time of the ultrasonic signals emanating from the transducers through the pipe walls. The relationship between the speed of sound and the α and θ are expressed by Snell's law as

$$\frac{\sin\alpha}{c_{\mathrm{m}}} = \frac{\sin\theta}{c_{\mathrm{f}}}, \tag{2}$$

where c_{m} is the speed of sound in the ultrasonic transducers. Based on Eqs. (1) and (2), the line-averaged velocity, V_{L}, can be expressed as:

$$\Delta t = 2D\tan\theta\left(\frac{V_{\mathrm{L}}}{c_{\mathrm{f}}^2 - V_{\mathrm{L}}^2\sin^2\theta}\right), \tag{3}$$

where $\Delta t = T_2 - T_1$. The profile factor, PF, is used to convert the line-averaged velocity, V_{L}, into the flow rate, Q_{TOF}, as follows:

$$Q_{\mathrm{TOF}} = PF \cdot \frac{\pi D^2}{4} \cdot V_{\mathrm{L}} \tag{4}$$

In general, PF is determined based on the calibration considering the flow rate, upstream and downstream conditions, and so on. Therefore, the accuracy of Δt determination is important for the TOF flowmeters.

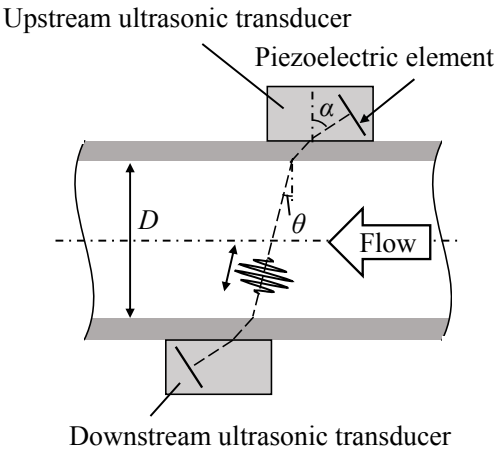

Fig.1 Schematic of a clamp-on ultrasonic flowmeter (top view).

3. Methodology

3.1 Experimental facility

Fig. 2 shows a schematic of the experimental facility used for two-phase (air–water) flow rate measurements using clamp-on TOF ultrasonic flowmeters. The experimental facility consisted of a two-phase flow mixing section, a flow visualization section, and a test section for ultrasonic signal transmission. The test section was installed horizontally in the experimental facility. A blower was used to generate the main air flow in the test section. The mixing section was constructed from an acrylic resin pipe (inner diameter: 130 mm, length: 150 mm) connected to reducers (SGP125A×50A) on both sides of the pipe. A fog spray nozzle (model: BIMJ2022, H.Ikeuchi & Co., Ltd., Japan) connected to a water pump (model: 10-LPM-610, Maruyama Manufacturing Co., Ltd., Japan) and an air compressor (model: GT-75K, Meiji Air Compressor Mfg. Co., Ltd., Japan) was installed at the mixing section. By varying the rate of air supply and water flow rate, the mean diameter of the droplets could be controlled

within a range of 30–60 μm with a fixed spray angle of 20°. Three types of flowmeters were used in this work: (1) a vortex flowmeter (model: VXW1050-N11G-1104A, OVAL Corporation, Japan) with an accuracy of 1% of the full scale to measure the air flow rate from the blower, (2) a mass flowmeter (model: SEF-12, HORIBA STEC Co., Ltd., Japan) with an accuracy of ±3% of the full scale to measure the air flow-rate from the compressor, and (3) an impeller flowmeter (model: ND05-TATAAA-RD, Aichi Tokei Denki Co., Ltd., Japan) with an accuracy of ±2% of the reading scale to measure the water flow rate. The flow visualization section was made of an acrylic resin pipe with an inner diameter of 50 mm and length of 1.5 m. An SGP50A carbon steel pipe (outer diameter: 60.5 mm, inner diameter: 52.9 mm, length: 1.0 m) was placed downstream of the flow visualization section. A high-speed camera (model: FASTCAM SA 1.1, Photron Limited, Japan) with a frame rate of 10,000 frames per second and shutter speed of 1/25,000 was employed to classify the flow regimes of the two-phase flows.

The water flow rate was varied from 0.30 to 1.35 L/min, which corresponds to a superficial water velocity, J_L, range of 0.0023–0.0100 m/s. The air flow rates were varied within a range of 1380–3830 L/min and 130–160 L/min for the blower and air compressor, respectively. The ratios of the air flow rates from the compressor and blower were within a range of 0.035–0.116. The total air flow rate was varied from 1540 to 3990 L/min, which corresponds to a superficial air velocity, J_G, of 11.7–30.2 m/s. The wetness fraction, β, was varied between 0 and 23% and is defined as

$$\beta = \frac{\rho_L J_L}{\rho_L J_L + \rho_G J_G}, \tag{5}$$

where ρ_L and ρ_G are the water and air densities, respectively. The experimental conditions for two-phase

flow were selected based on the conditions in steam pipe lines. An open-to-atmosphere separator tank was used in the experimental facility and the experiments were carried out under atmospheric pressure conditions at a temperature of 20–22°C.

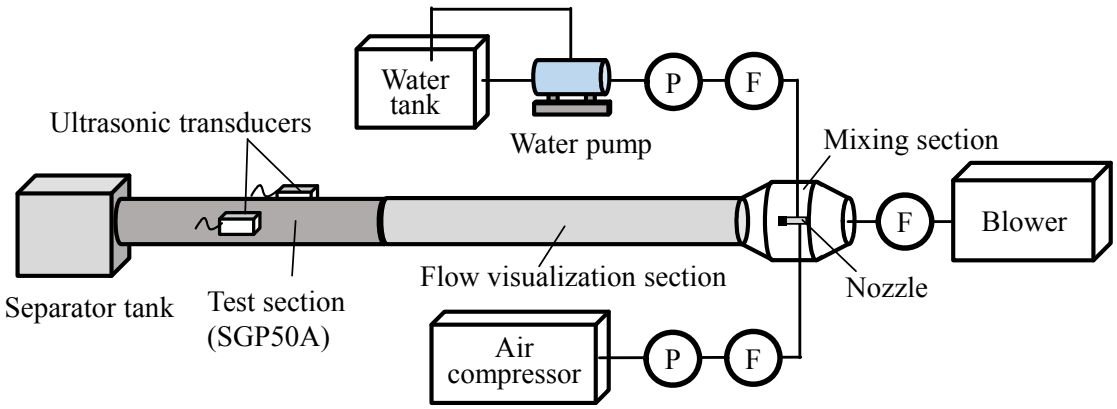

Fig. 2 Schematic of the experimental facility.

3.2 Experimental procedure

Two ultrasonic transducers were attached horizontally to the outer surface of the test section (opposite to one another), as shown in Fig. 3. In general, most of the ultrasonic signals will propagate not only through the flow but also through the pipe wall as guided waves. These guided wave are one of the noise sources, which complicates the detection of the ultrasonic signals propagating through the flow. In order to minimize the generation of guided waves, butyl rubber was used as a damping material and was affixed to the outer surface of the test section. The incidence angle between the ultrasonic signal and pipe wall was 57°. The angle between the wedge and pipe surface was greater than the critical angle. Thus, the ultrasonic wave did not propagate in the pipe wall as a body wave and formed wider beams in

the pipe. The transducers employed for the measurements were the same as those used by Sasaki et al. [13].

The ultrasonic transducers were connected to a pulser/receiver (model: JPR-10C-2CH-KB, Japan Probe Co. Ltd., Japan). Four-cycle burst signals at 1 MHz were emitted as the ultrasonic signals. Both of the ultrasonic transducers had the same center frequency of 1 MHz. The ultrasonic pulses were periodically emitted from the transducers at a pulse repetition frequency of 100 Hz. The ultrasonic signals were received at the opposite transducer and sampled using a high-speed digitizer (model: NI PXI-5114, National Instruments Corporation, USA) with a sampling rate of 250 MS/s (mega-samples per second). Five hundred waves were continuously recorded and the measurements were repeated 10 times, resulting in 5,000 ultrasonic signals in each direction: from the upstream transducer to the downstream transducer and vice versa. Using the consecutive signals, $V(i, t)$, the ensemble-averaged signals $\overline{V}(t)$ and standard deviations $V_{\mathrm{std}}(t)$ were calculated in each direction as

$$\overline{V}(t)=\frac{1}{N}\sum_{i}^{N}V(i,t) \tag{6}$$

$$V_{\mathrm{std}}(t)=\sqrt{\frac{1}{N}\sum_{i=1}^{N}\left(V(i,t)-\overline{V}(t)\right)^2} \tag{7}$$

where N is the number of waves for averaging; i is the pulse number; t is the elapse time from each pulse emission; and V is the wave signal obtained at A/D board.

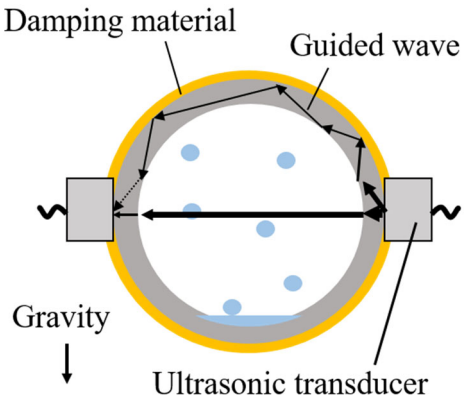

Fig. 3 Schematic of the test section (front view).

4. Results and discussion

4.1 Flow visualization

Fig. 4 shows the flow visualization results of the two-phase flow at different superficial air velocities, J_G, and superficial water velocities, J_L. The wetness fraction, β, was 19%. The vertical positions of the ultrasonic transducers installed downstream of the flow visualization section for each test case is indicated by the dashed box in each image. It can be observed that most of the droplets flowed like a cloud in the pipe for all test cases. In addition to the droplets, most of the liquid flowed along the bottom of the pipes when J_G = 11.2 m/s and J_L = 0.0030 m/s (Fig. 4(a)). In this case, fluctuations at the liquid-gas interface were not significant and the flow was classified as stratified flow. The void fraction can be estimated at 95% based on the height of the liquid phase obtained from the pictures, assuming that surface of the liquid phase is smooth and flat [20]. When J_G = 15.6 m/s and J_L = 0.0045 m/s (Fig. 4(b)), numerous large droplets were observed at the pipe wall and these droplets flowed

to downstream. There was no liquid film observed at the pipe wall except at the bottom of the pipe. A wavy liquid-gas interface was present and therefore, the flow regime was classified as wavy flow. At higher values of J_G and J_L (Figs. 4(c)–(e)), the liquid film covered all over the pipe wall, as indicated by the light and dark regions in the images. In these cases, the flow was classified as annular mist flow, and there was significant movement of the liquid film between the bottom and top of the pipe. There have been several investigations for predicting the void fraction in horizontal two-phase flow. The void fraction in wavy and annular mist flows in the experimental conditions can be estimated at more than 98% based on a slip ratio model with Lockhart & Martinelli correlation [21]. A flow regime map was plotted based on these visual observations, as shown in Fig. 5. The empirical models of Weisman et al. [22] for wavy–stratified transition and annular transition are also indicated in the figure and are given by

$$\left(\frac{\sigma}{gD^2(\rho_L-\rho_G)}\right)^{0.20}\left(\frac{DG_G}{\mu_G}\right)^{0.45}=8(J_G/J_L)^{0.16} \quad \text{for wavy–stratified transition}$$

$$1.9(J_G/J_L)^{1/8}=\mathrm{Ku}^{0.2}\mathrm{Fr}^{0.18}=\left(\frac{J_G\rho_G{}^{1/2}}{[g(\rho_L-\rho_G)\sigma]^{1/4}}\right)^{0.2}\left(\frac{J_G{}^2}{gD}\right)^{0.18} \quad (8)$$

for annular transition,

where σ denotes the surface tension; g denotes the acceleration due to gravity; μ denotes the fluid viscosity; G denotes the mass flux; Ku is the Kutateladze number; and Fr is the Froude number. Based on the results, the values of J_G and J_L for annular mist flow in the experiments showed good agreement with the empirical model for annular transition. However, the values of J_G and J_L for stratified flow were

confirmed to be in the wavy flow regime.

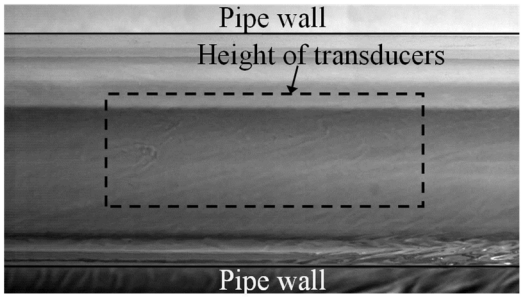

(a) J_G = 11.2 m/s, J_L = 0.0030 m/s

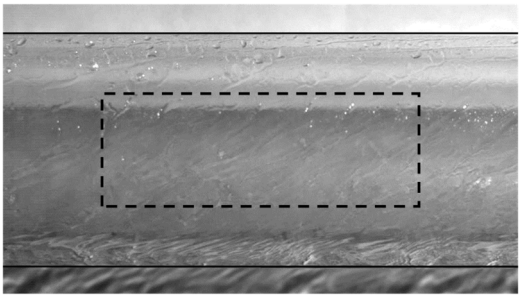

(b) J_G = 15.6 m/s, J_L = 0.0045 m/s

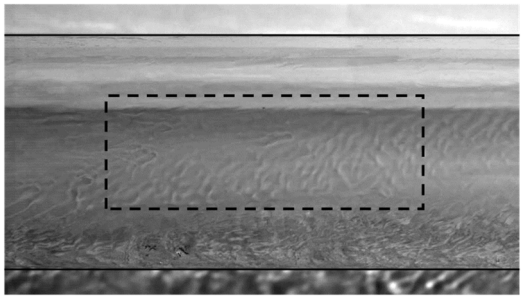

(c) J_G = 21.1 m/s, J_L = 0.0060 m/s

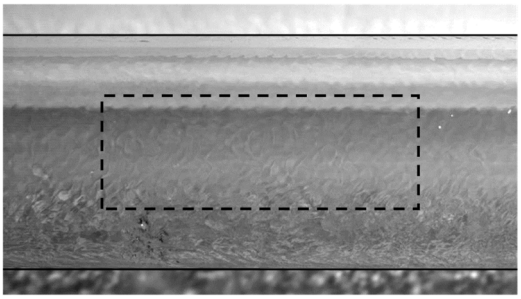

(d) J_G = 25.6 m/s, J_L = 0.0076 m/s

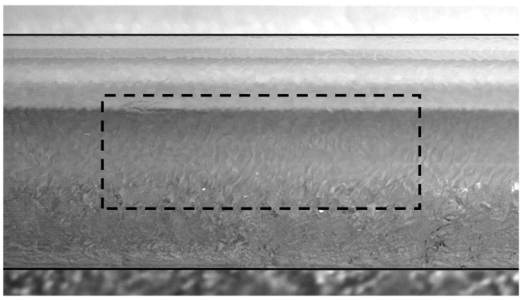

(e) J_G = 30.1 m/s, J_L = 0.0090 m/s

Fig. 4 Flow visualization results of the two-phase flow at different values of J_G and J_L, where β = 19%

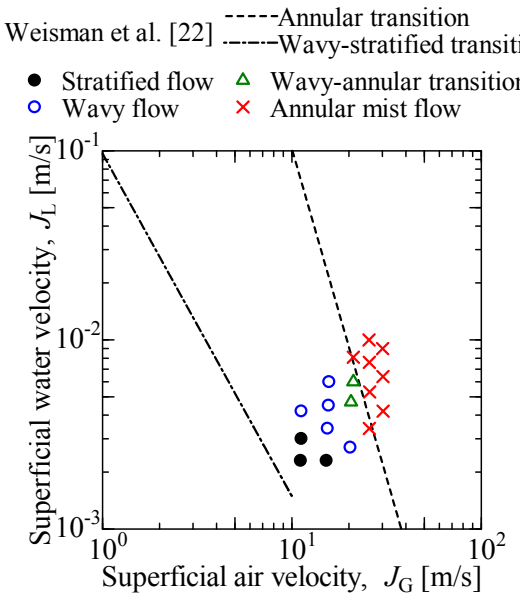

Fig.5 Flow regime map plotted based on the visual observations.

4.2 Characteristics of the transmitted ultrasonic signals

Fig. 6 shows the ensemble averaged transmitted ultrasonic signal and its standard deviations in stationary air. The number of waves, N, used for averaging was 500. The high intensities of the transmitted ultrasonic signal at the beginning of the elapsed time ($t < 5$ μs) represents the noise associated with the burst signals of the emitted pulse because the transmitter and receiver sensors were connected with the same pulser/receiver. Therefore, the signal is neglected. The presence of guided waves propagating in the pipe wall was detected at $t > 40$ μs. The ultrasonic signal transmitted through the stationary air was clearly detected at 190 μs, which was the target signal for the measurements. It shall be noted that the standard deviation should be 0 if the signal is not time-dependent. However, this was not the case because white noise was present in the ultrasonic signals due to measurement system. In general, the standard deviation of the transmitted ultrasonic signal was almost invariant with respect to

time.

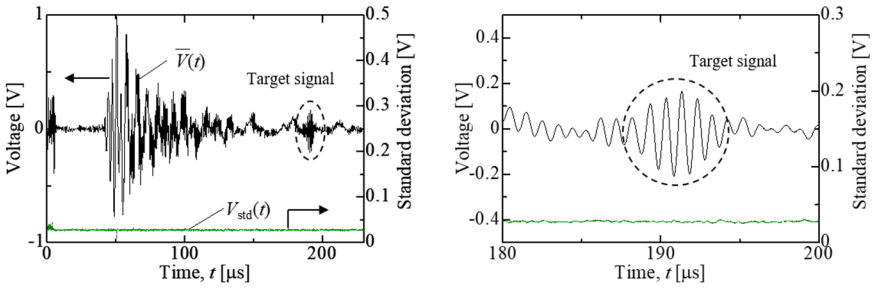

Fig. 6 Ensemble-averaged transmitted ultrasonic signal and its standard deviations in stationary air (N = 500).

Fig. 7 shows the ensemble-averaged ultrasonic-signals transmitted from the upstream and downstream ultrasonic transducers and their standard deviations in single-phase (air) flows for different area-averaged velocity, $\overline{u}$. The transmitted ultrasonic signals were averaged based on 5,000 waves. It can be observed that the transit time difference between the upstream and downstream ultrasonic transducers, Δt, increased with an increase in $\overline{u}$. In contrast, the intensity of the target signal decreased with an increase in $\overline{u}$, which can be attributed to the higher attenuation of ultrasonic signals as a result of turbulence dissipation. Therefore, the higher the area-averaged velocity, the lower the intensity of the transmitted ultrasonic signal. This indicates that it is more difficult to accurately estimate Δt based on the transmitted ultrasonic signals at higher flow velocities. The standard deviations of the transmitted ultrasonic signals in theses test cases were similar to those in stationary air except at the target signals. The standard deviations at the target signals create a convex shape, with a frequency of ~2 MHz. There

were slight variations in the instantaneous line-averaged velocity along the ultrasonic beam with an increase in $\bar{u}$ because of flow turbulence, which led to differences in the transit time between the upstream and downstream ultrasonic signals [5]. Therefore, the maximum standard deviations at the target signal slightly increased with an increase in $\bar{u}$. Because the ultrasonic pulses were burst signals with a center frequency, f_0, of 1 MHz, it can be ascertained that the standard deviations with a frequency of ~2 MHz were due to differences in the transit time of the ultrasonic pulses.

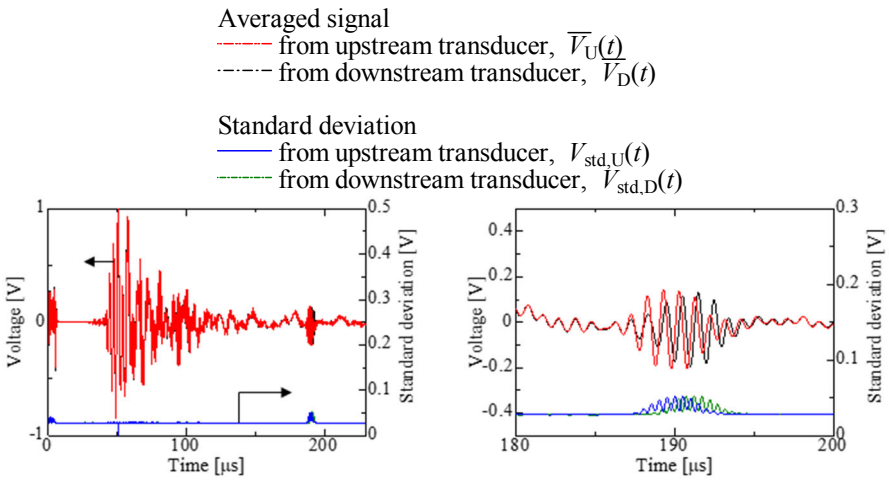

(a) $\overline{u}$ = 10.1 m/s

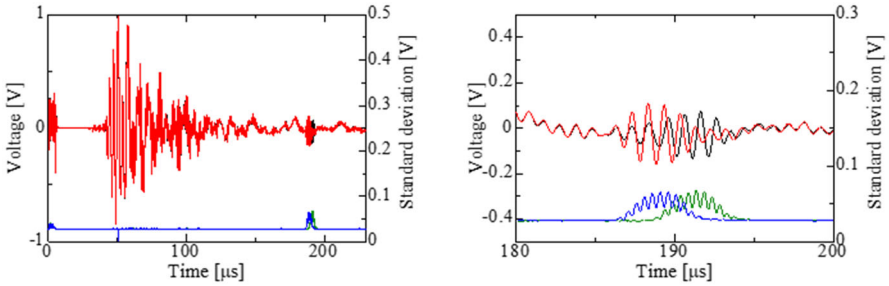

(b) $\overline{u}$ = 20.0 m/s

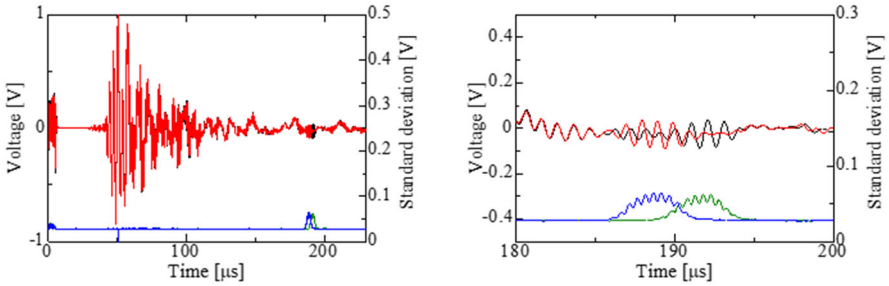

(c) $\overline{u}$ = 29.1 m/s

Fig. 7 Ensemble-averaged ultrasonic signals transmitted from the upstream and downstrem ultrasonic transducers and their standard deviations in single-phase (air) flow (N = 5,000) for different values of $\overline{u}$.

Figs. 8 show the ensemble-averaged ultrasonic signals transmitted from the upstream and downstream ultrasonic transducers and their standard deviations in two-phase (air–water) flows for different superficial air velocities, J_G, and superficial water velocities, J_L, where β = 19% (Fig. 8). The target signals were confirmed at t = 190 μs and the standard deviations at the target signals form a convex shape, similar to those in single-phase (air) flows. However, there were significant differences in the standard deviations during the guided wave period, depending on the flow regime, even though the ensemble-averaged signal patterns were similar. In stratified flow (Fig. 8(a)), the standard deviations were almost constant except at the onset of the guided wave (t < 100 μs). The standard deviations during the guided wave period increased when the flow regime transitioned from wavy to annular mist flow. In annular mist flow (Figs. 8(d)), the intensities of the target signals were significantly lower compared to those in other flow conditions (Figs. 8(a)–(c)) whereas the standard deviations during the guided wave period were significantly higher. Although a small gap at the pipe connection between the visual observation and the ultrasonic test sections existed, the distributions of standard deviation were related to the flow regime observation. Therefore, it can be thought that the small gap was not so significant for the flow regime. In addition, it was confirmed that the standard deviations at the target signals create a typical distinctive pattern. Therefore, it can be deduced that the target signals can be easily distinguished from the noisy signals based on the standard deviations of the transmitted ultrasonic signals compared with the ensemble-averaged signals.

It can also be observed that the high-intensity guided waves appeared randomly for each test case. This indicates that some of the guided waves in the pipe wall are transmitted to the liquid film at the internal pipe wall and the waves are reflected at the liquid-gas interface. If there are no fluctuations at the liquid-gas interface, there will be no changes in the propagation paths of the guided waves, which will lead to low standard deviations. In contrast, if there are large fluctuations at the liquid-gas interface, random reflection will occur at the interface and thus, the propagation paths of the ultrasonic signals will change instantaneously. In this case, some of the reflected ultrasonic signals will be transmitted through the pipe wall and converted into guided waves. As the standard deviations in upstream and downstream directions were almost the same during guided-wave period in each flow regime, it can be assumed that the upstream and downstream sensors were mounted almost axisymmetrically with respect to the vertical axis. In contrast, if the upstream and downstream sensors are not in the correct positions, *i.e.* not axisymmetric with respect to the two-phase flows, the values of the standard deviations may be different.

Fig. 9 show the standard deviations for different values of β, at the same value of J_G under wavy and annular mist flow regimes. In wavy flow, changes in the propagation path were mainly caused by the fluctuations in the liquid–gas interface flowing along the bottom of the pipes. Thus, the standard deviation slightly increased with the wetness fraction. In annular mist flow, fluctuation in the liquid film substantially alters the paths of ultrasonic propagation. This effect mainly appeared around 100 μs in the transit time. The maximum values of the standard deviation increased significantly with

β. If multiple reflections occur at the liquid–gas interfaces, the propagation distances of the guided wave increase, resulting in the longer propagation times. With increase in the number of reflections on the liquid–gas interface, ultrasonic attenuation at the interface also increases. Thus, the intensity of the guided wave decreases with increasing transit time, t. Decreases in the standard deviation after t = 100 μs occurred more rapidly at higher β. As a result, there are conditions that the standard deviation at the target signal, t = 190 μs, became lower for higher β. Therefore, the standard deviation distribution is dependent on the flow regime and fluctuations at the liquid–gas interface. However, the transit time that results in the maximum value of the standard deviation may change with the size of the pipe, liquid film thickness, and covered area on the wall. These observations necessitate further investigations. In contrast, the minute liquid droplets may disturb the propagation paths of the ultrasonic signals in the flow. It is very likely that the intensities of the target signals propagating in the flow will weaken with an increase in the number of liquid droplets. However, the differences due to the wetness fraction are not as pronounced compared with those due to changes in the flow regime. The volume ratio of liquid droplets in the gas phase along the measurement line could be estimated considerably less than 0.1%. Furthermore, the wider ultrasonic beam was used for the measurement. Therefore, the disturbance in the ultrasonic propagation caused by the droplets was not significant. Thus, the generation of random guided waves associated with the fluctuations at the liquid–gas interface is a significant factor that reduces the SNR of the target signal.

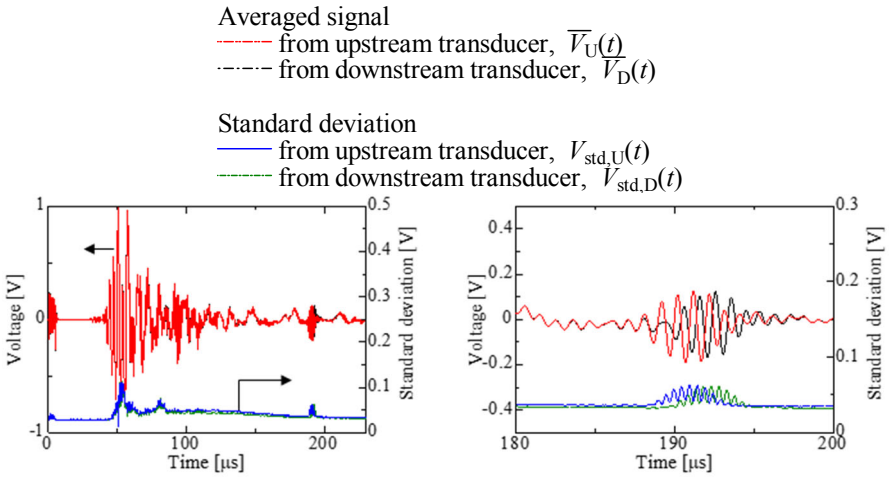

(a) Stratified flow: J_G = 12.3 m/s, J_L = 0.0030 m/s

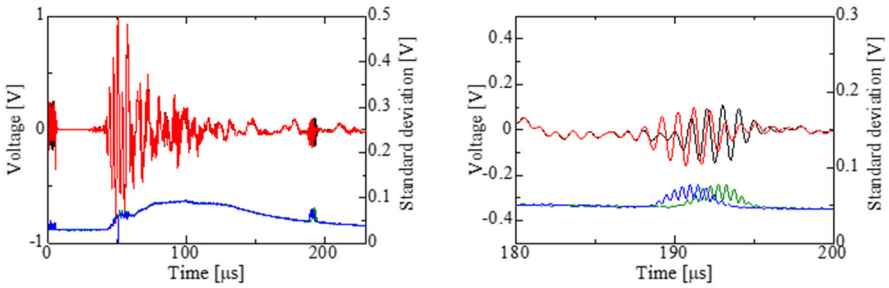

(b) Wavy flow: J_G = 15.8 m/s, J_L = 0.0046 m/s

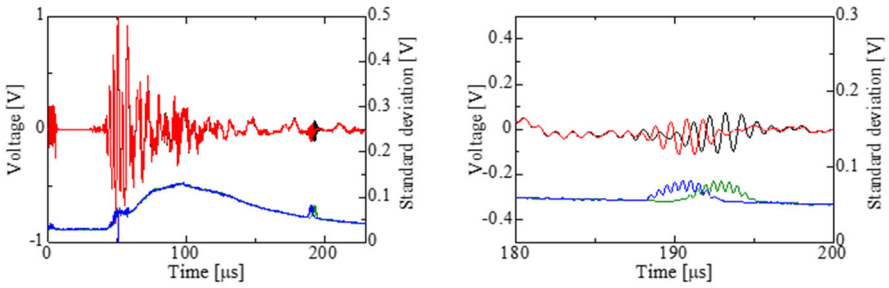

(c) Wavy–annular transition: J_G = 21.5 m/s, J_L = 0.0061 m/s

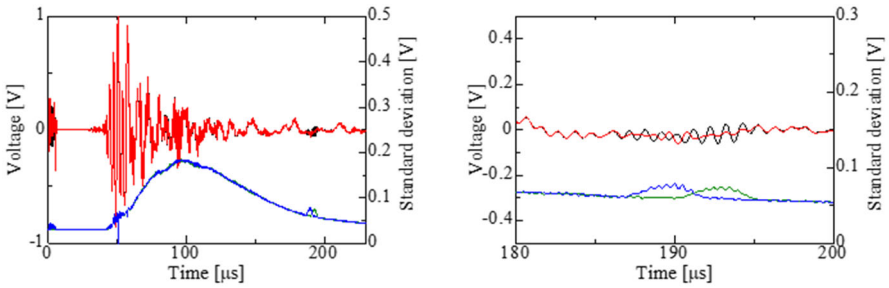

(d) Annular mist flow: J_G = 30.8 m/s, J_L = 0.0091 m/s

Fig. 8 Ensemble-averaged ultrasonic signals transmitted from the upstream and downstream ultrasonic transducers and their standard deviations in two-phase (air–water) flows for different values of J_G and J_L, where β = 19% (N = 5,000).

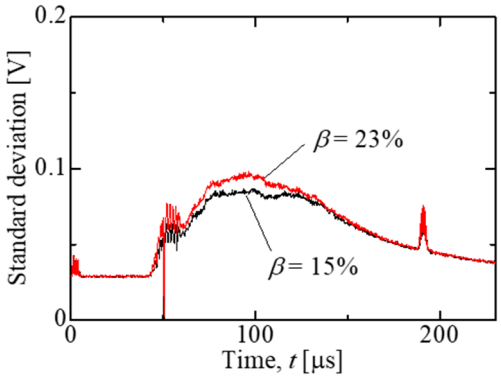

(a) Wavy flow: J_G = 15 m/s

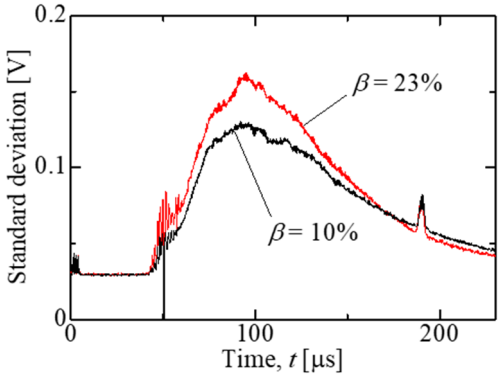

(b) Annular mist flow: J_G = 25 m/s

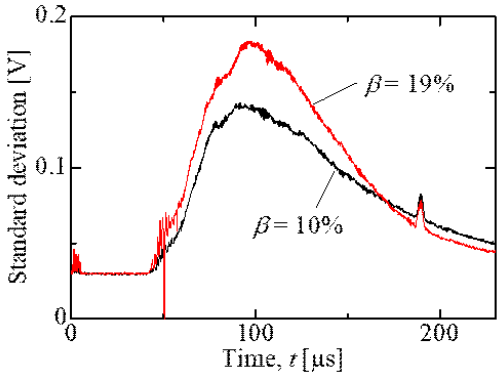

(c) Annular mist flow: J_G = 31 m/s

Fig. 9 Comparison of standard deviations in two-phase (air–water) flows for different values of β under wavy and annular mist flow regimes at the same J_G (N = 5,000).

4.3 Calculation of the time-of-flight

Several methods have been developed to determine the transit time difference between the ultrasonic signals transmitted from the upstream and downstream transducers, Δt, [23] such as the trigger method based on a fixed threshold and the cross-correlation method. In these methods, it is of utmost importance to distinguish the target signals from the noisy signals accurately. In this study, the normalized cross-correlation function, $R(\tau)$, was used to estimate Δt, as follows:

$$R(\tau) = \frac{\int E_{\mathrm{U}}(t) E_{\mathrm{D}}(t+\tau) dt}{\sqrt{\int E_{\mathrm{U}}(t)^2 dt \int E_{\mathrm{D}}(t+\tau)^2 dt}} \tag{9}$$

where the E_{U} and E_{D} represent the signals, that is, $\overline{V}(t)$ or $V_{\mathrm{std}}(t)$, received from the upstream and downstream ultrasonic transducers, respectively. The value of τ at which $R(\tau)$ is maximum is defined as Δt.

Fig. 10 shows the relationship between the transit time difference, Δt, and area-averaged velocity, $\overline{u}$, in single-phase (air) flows calculated using the ensemble-averaged ultrasonic signals shown in Fig. 7. The least squares approximation and uncertainty range of the reference flowmeter are also indicated in Fig. 10. As c_{f}^2 is much larger than $V_{\mathrm{L}}^2 \sin^2\theta$, Δt increases almost linearly with an increase in $\overline{u}$ as indicated in Eq. (3). In addition, the data were well within the uncertainty range of the reference flowmeter.

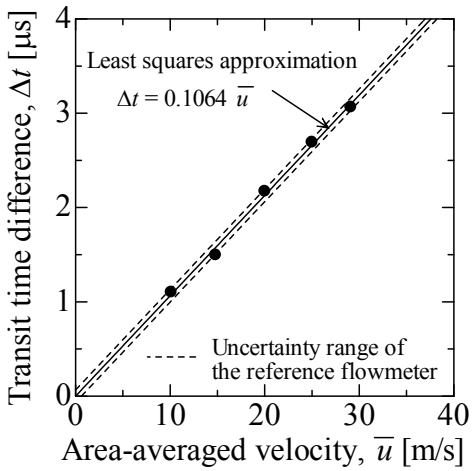

Fig. 10 Relationship between $\overline{u}$ and Δt in single-phase (air) flows (N = 5,000).

Fig. 11 shows the transit time difference, Δt, calculated based on 50 averaged ultrasonic signals for different superficial air velocities, J_G, and superficial water velocities, J_L, where β = 19%. Thus, 100 results of Δt were obtained from 5,000 waves for each test case. The reference values, Δt_{Ref}, were calculated using least squares approximation for single–phase (air) flows, assuming that the change in gas velocity due to liquid present in two-phase (air–water) is within uncertainty range of the reference flow meter. It can be seen from Figs. 11(a) and (b) that the Δt values conform well with the reference values. In contrast, there was a significant difference in Δt determined from the ensemble-average ultrasonic signals and reference values when J_G = 21.5 m/s, and J_L = 0.0061 m/s (Fig. 11(c)) due to the lower SNR. In Fig. 11(c), several misdetections of Δt were confirmed in the 100 data. The differences are approximately 1 μs from the reference value. In the cross-correlation function, the shapes of the target signals from the upstream and downstream transducers are compared to calculate Δt. As the burst

signal was used for the measurements (Fig. 8), misdetection of Δt in the cross-correlation function is likely to have occurred at $\Delta t_{\mathrm{Ref}} \pm n/f_0$, where n is an integer. In this study, with decreasing SNR, misdetection of Δt likely occurred at $\Delta t_{\mathrm{Ref}} \pm n$ [μs] with f_0 = 1 MHz. As shown in Fig. 7, for single-phase flow, the intensity of the transmitted signal decreased with the gas velocity. In addition to the higher noises, the intensity of the transmitted signal was low. As a result, it was difficult to determine Δt accurately when J_{G} = 30.8 m/s and J_{L} = 0.0091 m/s (Fig. 11(d)). To confirm the misdetections of Δt at $\Delta t_{\mathrm{Ref}} \pm n/f_0$, the threshold was set at $\Delta t_{\mathrm{Ref}} \pm 0.5$ μs. If Δt was within $\Delta t_{\mathrm{Ref}} \pm 0.5$ μs, it was considered to have been successfully obtained. Fig. 12 shows the success ratios, R, of determining the transit time difference, Δt, for different values of J_{G} and J_{L}. The empirical models of Weisman et al. [22] for wavy–stratified transition and annular transition are also plotted in the figure. It is apparent that the success ratios of determining Δt are the least for annular mist flows, where $R < 0.8$. This indicates that it is difficult to obtain accurate flow rate measurements at lower SNRs, as shown in Figs. 8(d) and 9(b).

As shown in Figs. 8 and 9, the peaks of the standard deviations of the target signals can be clearly observed even in annular mist flows. Thus, it is confirmed that the transit time difference values, Δt, can be determined based on the standard deviations of the ultrasonic signals. Fig. 13 shows the comparison of the cross-correlation coefficients $R(\tau)$ determined based on ensemble-averaged ultrasonic signals and standard deviations of the target signals (N = 5,000). To obtain a more accurate estimate of Δt, the maximum $R(\tau)$ must be sufficiently large. It shall be noted that τ corresponding to the maximum $R(\tau)$ is Δt. The determined Δt and reference value are shown as vertical lines in the

figures. It can be observed from Fig. 13 that the $R(\tau)$ values determined based on the ensemble-averaged ultrasonic signals and standard deviations of the target signals fluctuates at 1 and 2 MHz, respectively, due to differences in the signal shape. The difference in τ at which $R(\tau)$ was maximum was found to be small at higher SNRs (Figs. 13(a) and (b)) such that the maximum $R(\tau)$ values overlap one another. However, the difference in τ corresponding to the maximum $R(\tau)$ obtained based on the ensemble-averaged ultrasonic signals and standard deviations of the target signals was significant at a lower SNR, as shown in Fig. 13(c). In this case, the value of τ determined based on the standard deviations of the target signals showed good agreement with the reference value. Furthermore, the distribution of the cross-correlation coefficients obtained based on the standard deviations of the target signals tends to have a single well-defined peak, which facilitates in identifying the maximum $R(\tau)$. As shown in Figs. 8 and 9, ensemble-averaged ultrasonic signals of the target signals changes from burst wave into the distorted wave with a decrease in the SNR, making it difficult to distinguish the target signal from the noisy signal, resulting in an inaccurate estimation of Δt. In contrast, the standard deviations of the target signal follow a typical distinctive convex pattern, which facilitates in identifying the true target signal. Hence, it is possible to obtain a more accurate estimate of Δt based on the standard deviations of the target signals.

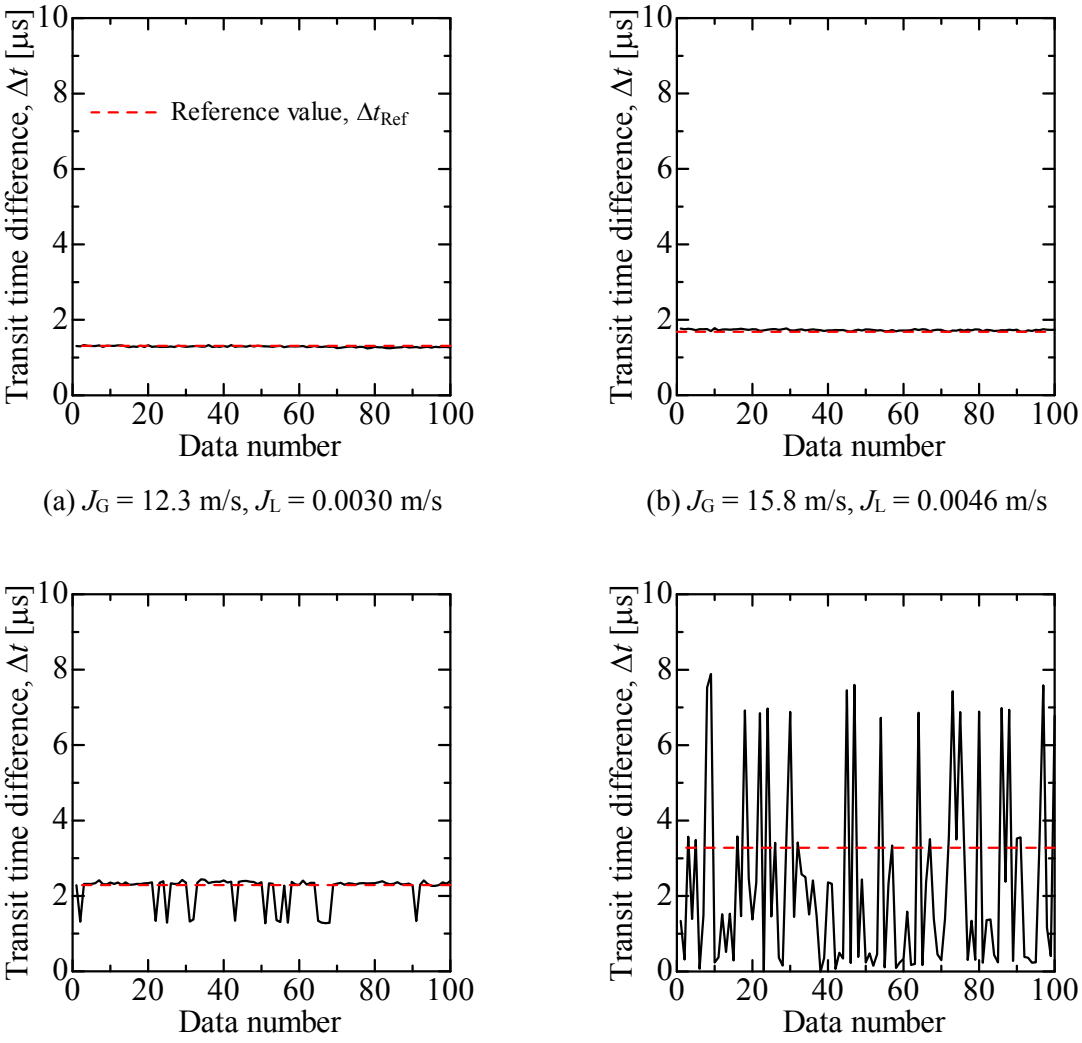

(a) J_G = 12.3 m/s, J_L = 0.0030 m/s

(b) J_G = 15.8 m/s, J_L = 0.0046 m/s

(c) J_G = 21.5 m/s, J_L = 0.0061 m/s

(d) J_G = 30.8 m/s, J_L = 0.0091 m/s

Fig. 11 Comparison between the Δt determined from ensemble-averaged ultrasonic signals (N = 50) and the reference values for different values of J_G and J_L, where β = 19%.

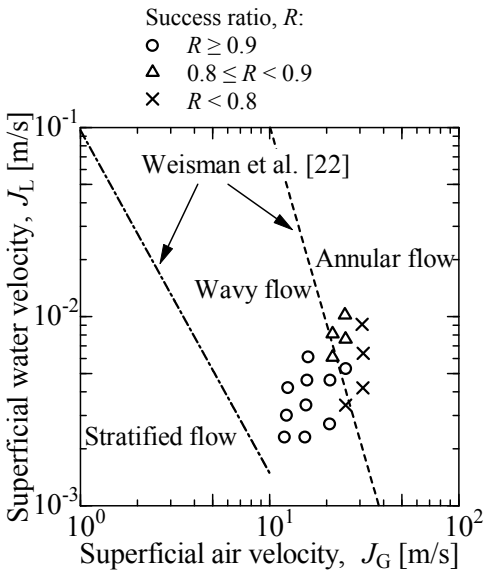

Fig. 12 Success ratios of determining Δt based on the ensemble-averaged ultrasonic signals ($N = 50$) for different values of J_G and J_L.

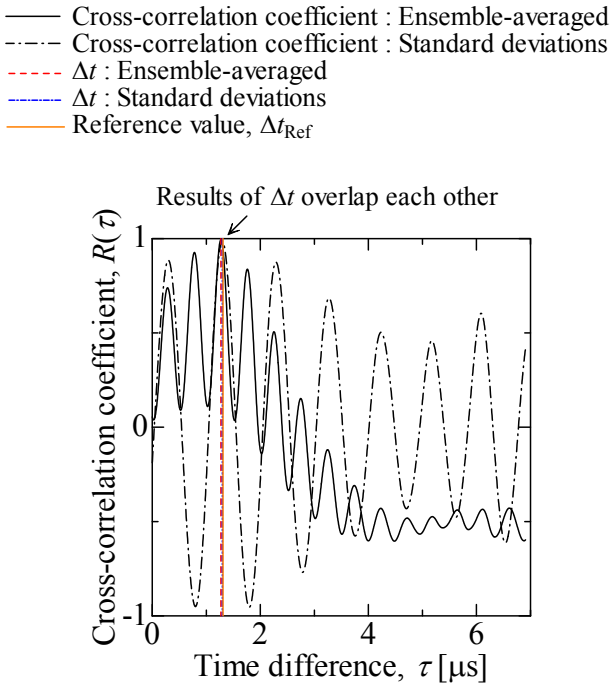

(a) J_G = 12.3 m/s, J_L = 0.0030 m/s

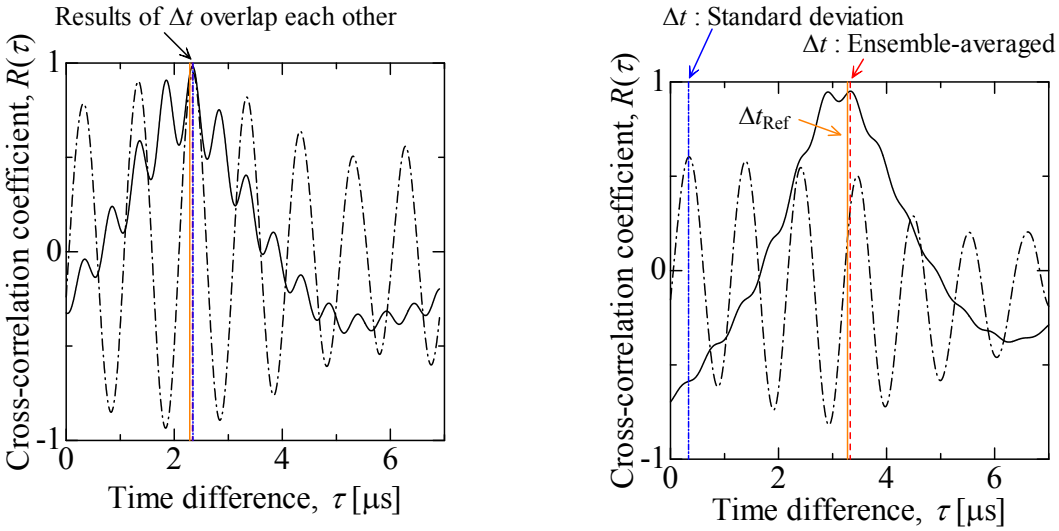

(b) J_G = 21.5 m/s, J_L = 0.0061 m/s

(c) J_G = 30.8 m/s, J_L = 0.0091 m/s

Fig. 13 Comparison of $R(\tau)$ determined from ensemble-averaged ultrasonic signals and standard deviations of the target signals (N = 5,000).

Fig. 14 shows the relationships between Δt and J_G, in two-phase (air–water) flows for different values of β. Here, Δt was determined based on the ensemble-averaged ultrasonic signals and standard deviations of the target signals as shown in Fig. 13. The solid lines refer to the reference values obtained for single-phase (air) flows. Increasing the number of waves used for averaging from 500 to 5,000 improved the accuracy of Δt determined based on the ensemble-averaged ultrasonic signals with a success ratio of 80–90%, as shown in Fig. 12. However, there was a significant difference in the Δt from the reference values at lower SNRs (where $R < 80\%$), as shown in Fig. 14(a). This indicates that increasing the number of waves for averaging does not improve the estimation accuracy of Δt at lower SNRs, regardless of the wetness fraction. It should be noted that the difference between the reference value and the measured data at $J_G = 25.2$ m/s with $\beta = 10\%$ is almost 1 μs, which corresponds to the period of the ultrasonic frequency. It means that misdetection of Δt in the cross-correlation occurred as discussed in Fig. 11. However, results for the other values of β at the same J_G agree well with the reference value. As discussed in Fig. 9, the standard deviation at $\beta = 10\%$ was slightly higher than that at higher β values with the same J_G. Due to the slight difference in the SNR, Δt could not be accurately obtained at $\beta = 10\%$ in $J_G = 25.2$ m/s. In contrast, the Δt values determined based on the standard deviations of the target signals showed good agreement with the reference values for all wetness fractions, as shown in Fig. 14(b). This indicates that this new approach can be useful to estimate the transit time difference at lower SNRs. However, the main disadvantage of the standard deviation

approach is that a large number of waves are required to determine the Δt compared to the ensemble-averaged approach. In other words, it is not possible to accurately determine Δt based on the standard deviations of the target signals if the number of waves is insufficient for the calculations.

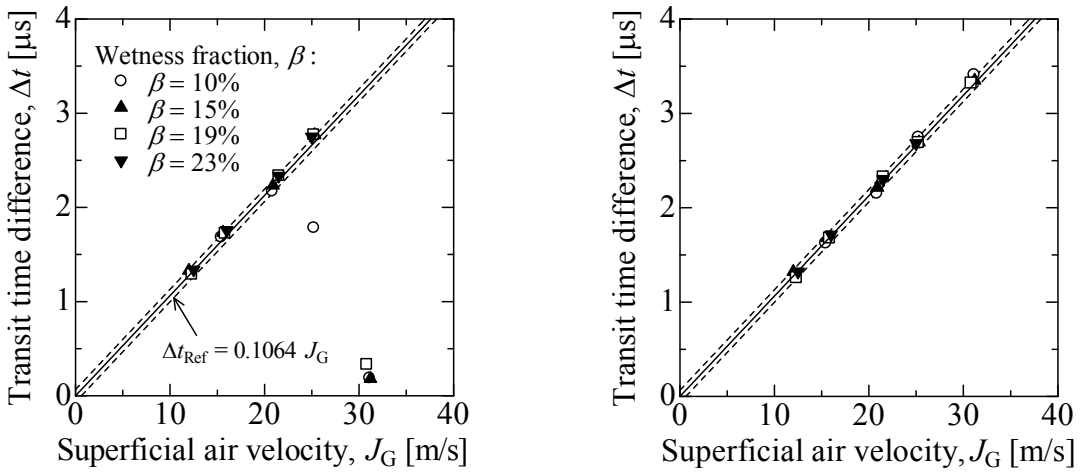

(a) Calculated based on ensemble-averaged ultrasonic signals

(b) Calculated based on standard deviations of the target signals

Fig. 14 Relationship between Δt determined from ensemble-averaged ultrasonic signals and standard deviations of the target signals (N = 5,000) and J_G in two-phase (air–water) flows.

5. Conclusions

In this study, a new signal processing method based on the standard deviation was proposed to improve the estimation accuracy of the transit time difference of clamp-on TOF ultrasonic flowmeters for wet steam flows.

The ultrasonic signals were found to be time-dependent and their characteristics vary depending on the flow regime. The generation of random time-dependent guided waves in the pipe wall was determined to be a significant factor that reduces the SNR of the target signal, which in turn, reduces

the success ratio of the transit time difference estimations. The guided waves in the pipe wall are transmitted to the liquid film and reflected at the liquid–gas interface, which alters the propagation path of the ultrasonic signals, resulting in noisy signals. The presence of noise in the ultrasonic signals makes it difficult to distinguish the target signal from the noisy signal, which affects the estimation accuracy of the transit time difference. The effect of guided waves on the ultrasonic signal propagation was more pronounced compared with the effect of liquid droplets. The success ratio of the transit time difference estimations decreased with an increase in the temporal change of the guided waves. In order to improve the estimation accuracy of the transit time difference, the cross-correlation coefficients should be determined based on the standard deviations of the target signals rather than ensemble-averaged ultrasonic signals. The results showed that the transit time difference can be determined accurately based on the standard deviation approach even for annular mist flows where the SNR is greatly reduced. The results also showed that the SNR of the ensemble-averaged target signal decreased as the effect of the guided waves became more significant. In contrast, the SNRs were significantly higher for the standard deviations of the target signals compared with those for ensemble-averaged target signals. Therefore, the standard deviation approach can be used to obtain a more accurate estimate of the transit time difference in cases where the SNR is reduced because of signal attenuation such as in wet steam flows. Furthermore, the standard deviation distribution varied significantly when the flow regime transitioned from stratified flow to annular mist flow and thus, the flow regime can also be roughly estimated based on the standard deviation distribution.

Acknowledgment

The authors are grateful to Dr. Hayashi and Mr. Sasaki (Azbil Corporation) for the fruitful discussions and advice on the ultrasonic sensors and settings.

References

[1] H. Zhoua, T. Jia, R. Wang, X. Ge, X. Tang, S. Tang, Multipath ultrasonic gas flow-meter based on multiple reference waves, Ultrasonics 82 (2018), 145–152. https://doi.org/10.1016/j.ultras.2017.07.010

[2] R. Steven, A. Hall, Orifice plate meter wet gas flow performance, Flow Measurement and Instrumentation 20 (2009), 141–151. https://doi.org/10.1016/j.flowmeasinst.2009.07.001

[3] Lynnworth L.C. and Liu Y., Ultrasonic flowmeters: Half-century progress report, 1955–2005 2006; 44: e1371–e1378. https://doi.org/10.1016/j.ultras.2006.05.046

[4] H. Murakawa, E. Muramatsu, K. Sugimoto, N. Takenaka, N. Furuichi, A dealiasing method for use with ultrasonic pulsed Doppler in measuring velocity profiles and flow rates in pipes, Measurement Science and Technology 26 (2015) 085301 (11pp). https://dx.doi.org/10.1088/0957-0233/26/8/085301

[5] E. Muramatsu, H. Murakawa, K. Sugimoto, H. Asano, N. Takenaka, N. Furuichi, Multi-wave ultrasonic Doppler method for measuring high flow-rates using staggered pulse intervals, Measurement Science and Technology 27 (2016) 025303 (11pp). https://dx.doi.org/10.1088/0957-0233/27/2/025303

[6] E. Muramatsu, H. Murakawa, D. Hashiguchi, K. Sugimoto, H. Asano, S. Wada, N. Furuichi, Applicability of hybrid ultrasonic flow meter for wide-range flow-rate under distorted velocity profile conditions, Experimental Thermal and Fluid Science 94 (2018) 49–58. https://dx.doi.org/10.1016/j.expthermflusci.2018.01.032

[7] W. Liu, C. Tan, F. Dong, Oil-water two-phase flow velocity measurement with Continuous wave ultrasonic Doppler, Journal of Physics: Conf. Series 1065 (2018) 092019. https://dx.doi.org/10.1088/1742-6596/1065/9/092019

[8] D. Xiaoxiao, C. Tan, Y. Yuan, F. Dong, Measuring Oil-water Two-phase flow velocity with continuous wave ultrasound Doppler sensor and drift-flux model, IEEE Transactions on Instrumentation

and Measurement 65 (2016), 1098–1107. https://dx.doi.org/10.1109/TIM.2015.2507740

[9] D. Kurniadi, A. Trisnobudi, A multi-path ultrasonic transit time flow meter using a tomography method for gas flow velocity profile measurement, Part. Part. Syst. Charact 23 (2006) 330-380. https://dx.doi.org/10.1002/ppsc.200601067

[10] J.J.S. Shen, A new method of steam quality measurement based on ultrasound, Transactions of the ASME J. Energy Resour. Technol. 121 (1999) 172–175. https://doi.org/10.1115/1.2795978

[11] L. Xing, C. Hua, H. Zhu, W. Drahm, Flow measurement model of ultrasonic flowmeter for gas-liquid two-phase stratified and annular flows, Advances in Mechanical Engineering 2014 (2014) Article ID 194871. https://journals.sagepub.com/doi/10.1155/2014/194871

[12] H. Nishiguchi, T. Sawayama, K. Naganuma, A propagation time difference evaluation for a clamp-on ultrasonic flowmeter, Japanese J. Applied Physics 55 (2016) 07KB05. https://dx.doi.org/10.7567/JJAP.55.07KB05

[13] H. Sasaki, T. Hayashi, Development of a clamp-on ultrasonic flowmeter for gas, azbil Technical Review, Vol. April 2015 (2015) 63–69 (in Japanese).

[14] T. Hayashi, H. Sasaki, S. Umezawa, K. Sugita, Clamp-on ultrasonic steam flowmeter using transducer with supercritical angle and damping material with high temperature endurance, Proc. the 37th symposium on ultrasonic electronics 2016; #1P2-7.

[15] Z. Fan, W. Jiang, W.M.D. Wright, Non-contact ultrasonic gas flow metering using air-coupled leaky Lamb, Ultrasonics 89 (2018) 74–83. https://doi.org/10.1016/j.ultras.2018.04.008

[16] J. Doorhy, Strength in numbers: Matching Lamb wave sensors to the resonant frequency of a pipe wall, https://www.flowcontrolnetwork.com/strength-in-numbers/, 2012 (accessed 3 June 2019).

[17] H. Sasaki, T. Hayashi, S. Umezawa, K. Sugita, Steam flow measurement in the use of clamp-on method, Transactions of the JSME 83 (2017) 16-00397 (in Japanese).

https://dx.doi.org/10.1299/transjsme.16-00397

[18] R. Morita, F. Inada, Y. Uchiyama, S. Umezawa, M. Ishibashi, T. Funaki, Influence of steam wetness on steam flow rate measurement using ultrasonic flow meter, Transactions of the JSME 83 (2017) 16-00526 (in Japanese). https://dx.doi.org/10.1299/transjsme.16-00526

[19] R. Morita, Y. Uchiyama, S. Umezawa, K. Sugita, Measurement of wet steam flow rate by clamp-on type ultrasonic flow meter, Proc. of 22nd National Symposium of Power and Energy Systems (2017) #C134.

[20] T.-H. Ahn, B.-J. Yun, J.-J. Jeong, Void fraction prediction for separated flows in the nearly horizontal tubes, Nucl. Eng. Technol. 47 (2015) 669–677. http://dx.doi.org/10.1016/j.net.2015.06.005

[21] L. Xing, Y. Geng, C. Hua, H. Zhu, A. Rieder, W. Drahm, M. Bezdek, A combination method for metering gas–liquid two-phase flows of low liquid loading applying ultrasonic and Coriolis flowmeters, Flow Measurement and Instrumentation 37 (2014) 135–143. http://dx.doi.org/10.1016/j.flowmeasinst.2014.01.005

[22] J. Weisman, D. Duncan, J. Gibson, T. Crawford, Effects of fluid properties and pipe diameter on two-phase flow patterns in horizontal lines, Int. J. Multiphase Flow 5 (1979) 437–462. https://doi.org/10.1016/0301-9322(79)90031-4

[23] B. Liu, K.-J. Xu, L.-B. Mu, L. Tian, Echo energy integral based signal processing method for ultrasonic gas flow meter, Sensors and Actuators A 277 (2018), 181–189. https://doi.org/10.1016/j.sna.2018.05.019